Self-Powered Cardiac Pacemaker by Piezoelectric Polymer Nanogenerator Implant

Sara Azimi[a,b], Allahyar Golabchi[c,*], Abdolhossein Nekookar[d], Shahram Rabbani[e], Morteza Hassanpour Amiri[a], Kamal Asadi[a,f,*], Mohammad Mahdi Abolhasani[a,b,*]

[a] Max-Planck Institute for Polymer Research, Ackermannweg 10, 55128, Mainz, Germany

[b] Chemical Engineering Department, University of Kashan, 8731753153, Kashan, Iran

[c] Department of Cardiology, Cardiac Electrophysiology Center, Kashan University of Medical Sciences, 8715973474, Kashan, Iran

[d] Animal Core Facility, Reproductive Biomedicine Research Center, Royan Institute for Animal Biotechnology, ACECR, 16635148, Tehran, Iran

[e] Research Center for Advanced Technologies in Cardiovascular Medicine, Tehran Heart Center, Tehran University of Medical Sciences, 1417653761, Tehran, Iran

[f] Department of Physics, University of Bath, Claverton Down, Bath BA2 7AY, United Kingdom

[*]Corresponding authors: Allahyar Golabchi: golabchi@edc.mui.ac.ir
Kamal Asadi: asadi@mpi-mainz.mpg.de; ka787@bath.ac.uk
Mohammad Mahdi Abolhasani: abolhassani@mpip-mainz.mpg.de

Highlights

- A systematic optimization method has been employed to prepare a novel piezoelectric nanogenerator based on ternary PVDF composite fiber with outstanding power density.
- The encapsulated optimized nanogenerator is flexible and it has shown excellent biocompatibility.

- The *in vivo* implantation of the nanogenerator on the left ventricle of a dog animal model yields energy of 0.487 μJ, which is sufficient for the performance of a commercial pacemaker.
- A commercial pacemaker is powered by the optimized nanogenerator through *in vivo* energy harvesting, generating pacing pulses at the preset parameters.

Abstract

Self-powered biomedical implants improve the life of patients and lower the risks associated with battery replacement. Piezoelectric energy harvesters that generate electricity from the cardiac motions are among the potential candidates to be used in self-powered implants, such as cardiac pacemakers. In this context, lead-based ceramic piezoelectric nanogenerators (PNGs) were emerged, which are toxic and susceptible to fatigue crack, causing harms to the patients. Polyvinylidene fluoride-trifluoroethylene (PVDF-TrFE)-based films were also developed as cardiac energy harvesters. Here, we show a battery-free heart pacemaker that is powered by the generated electricity of a biocompatible and flexible piezoelectric polymer-based nanogenerator (PNG) from the cardiac motions of the left ventricle. The PNG is comprised of composite nanofibers of poly(vinilydine fluoride) (PVDF) and a hybrid nanofiller made of zinc oxide (ZnO) and reduced graphene oxide (rGO). The composite nanofiber is optimized towards achieving a large power output. *In vivo* implanted optimized PNG can successfully harvest 0.487 μJ from every heartbeat, which is conveniently larger than the pacing threshold energy for the human heart. The successful demonstration of a self-powered pacemaker places the polymer-based PNGs among the viable candidates for self-powered biomedical implants.

Keywords: PVDF composite fibers, piezoelectric nanogenerators, biomechanical energy harvesting, self-powered implantable medical electronics.

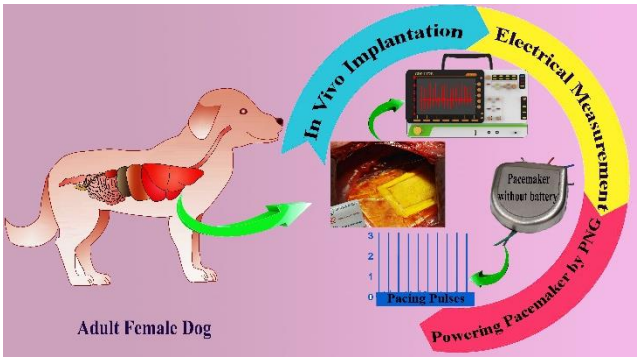

TOC Graphic

1. Introduction

Implantable medical electronics such as cardioverter defibrillators [1,2] and cardiac pacemakers [3] are remedy tools that improve the life of patients suffering from cardiovascular diseases. The health solutions, such as pacemakers, are typically battery-driven and have limited lifetime. The great progress in battery technology has extended the battery lifetime of a pacemaker up to 7 - 10 years. However, the additional surgery that is still needed to replace the device (or battery) poses major risk factors for the patients [4]. Self-powered medical implants can potentially overcome the battery replacement challenge, for instance through recharging the battery with the electricity that is harvested from the biomechanical energy from the movement of body organs such as cardiac motions.

During the last decade, piezoelectric nanogenerators (PNGs) [5-7] and triboelectric nanogenerators (TENGs) [8,9] have been in the center of attention owing to their significant capability to transform mechanical energy into electrical energy. PNGs have emerged as a simple solution to generate *in*

vivo and *in vitro* voltage from low frequency mechanical sources such as human activities [10,11] and cardiac motions [12-20]. The best performing piezoelectric materials are ceramics. However, the stringent requirement regarding flexibility and toxicity limits the application of lead-based piezoelectric ceramics [21,22].

Poly(vinilydine fluoride) (PVDF) is a semi-crystalline, flexible and biocompatible piezoelectric polymer [22] with five different polymorphs [23-26], of which the β and δ phases show the largest piezoelectric charge coefficient, d_{33} between -30 and -40 pV/m [27,28]. The piezoelectric PVDF films are commercially available but the power output of the film is very limited. Electrospinning of PVDF generates nanofibers that are readily poled in the piezoelectric β-phase and the performance of the PNGs is increased up to 4 times [29-33]. Nonetheless, the reported power of the comprising PNGs is still too low for driving the pacemaker. To increase the performance, composites of PVDF fibers containing nanofillers such as ceramic nanoparticles ($BaTiO_3$ [34], $NaNbO_3$ [35,36], and ZnO [37,38]) or carbon-based nanofillers (graphene [30,39] and carbon nanotube [40]) with the increased β-polymorph content have been developed. Recently, PVDF-based PNGs containing hybrid fillers have also been developed. For example, the output voltage from the PNG based on PVDF composite thin film containing ZnO and multi-walled carbon nanotubes has reached to 3.22 ± 0.24 V [17]. Energy harvester made with PVDF/Fe-rGO composite has provided open circuit voltage (V_{OC}) and short circuit current (I_{SC}) of 5.1 V and 0.254 μA by cyclic pressure, respectively [41]. PNG composed of PVDF composite fiber containing $BaTiO_3$-graphene has been reported to show nearly 4-fold increase in the V_{OC} compared to that of pristine PVDF fibers [42]. Karan et al. have fabricated PVDF/AlO-rGO-based PNG with a power density of 27.97 $\mu W/cm^3$ [43].

We propose that optimizing contents of hybrid nanofillers' components in the composite can lead to the formation of efficient electrospun PVDF composite fibers with even larger electrical power that can be eventually used for powering up medical implants with the goal of realizing self-powered implants.

Realization of self-powered implants such as heart pacemaker, would require integration of the PNG with the pacemaker and *in vivo* implantation. To that end, ceramic-based PNGs have been designed for biomechanical energy harvesting of cardiac motions in animals [12,13,19,20]. However, the proposed PNGs, despite their great promise, can cause harm to the patient because they are typically made of lead-based ceramics [22]. In addition, *in vitro* tests have been conducted to evaluate the biomechanical energy harvesting capability of polyvinylidene fluoride-trifluoroethylene (PVDF-TrFE)-based films through simulating the cardiac motion using shaker motor [16,17]. In the context of *in vivo* studies, PNGs fabricated from PVDF-TrFE films [14,15] and ZnO nanowire [18] have also been emerged as biomechanical energy harvesters of cardiac motions.

Here, we present an *in vivo* demonstration of a self-powered pacemaker in an animal model. The pacemaker is powered up by a biocompatible PNG through harvesting the biomechanical energy from the left ventricle, generating pacing pulses at the preset parameters. To realize the PNG, we have utilized the synergetic effects of ZnO and reduced graphene oxide (rGO) in enhancing the piezoelectric response of PNGs and synthesized an efficient hybrid filler for the development of a new generation of high performance PNGs.

In the following, we have employed a systematic study to prepare ternary composite of PVDF nanofibers with ZnO and rGO, wherein the amount of both nanofillers are optimized toward achieving the largest power output for low mechanical excitation frequency of 1 Hz. We have

shown that the PNG based on electrospun nanofibers of PVDF composite with only 0.1 wt% of ZnO:rGO (90:10 mass ratio) hybrid filler exhibits a nearly 10-fold increase in output voltage in comparison with that based on pristine PVDF nanofibers, delivering a large power density of 138 ± 2.82 μW/cm^3 under mechanical impact at 1 Hz and demonstrating high sensitivity parameter of 67.5 V/MPa. We have *in vivo* implemented the optimized PNG on a dog animal model. Sutured optimized PNG on the lateral wall of the left ventricle generates a maximum energy of 0.487 μJ, which is sufficient for the operation of commercial pacemakers. Demonstration of self-powered pacemakers, to the best of our knowledge for the first time using a flexible and biocompatible polymer-based PNG, opens new avenues towards further developments in self-powered implantable medical electronics.

2. Results and discussion

2.1. PNG optimization

As a benchmark, nanofibers of pristine PVDF are prepared first. The SEM images of the nanofibers (average diameters of 154 ± 38 nm) are given in Fig. 1a. The PNG from pristine PVDF nanofibers generates the V_{OC} and I_{SC} of 0.62 ± 0.03 V and 0.51 ± 0.01 μA (Supporting Information Fig. S7b-d), respectively, and a delivers maximum power density of 0.71 ± 0.06 μW/m^3 at an impact force of 20 N at 1 Hz, as shown in Fig. S8b (Supporting Information). To increase the power density, in the next step hybrid nanofibers of PVDF with ZnO flakes are prepared. Details of the ZnO synthesis, characterization and microstructural characterization of different PVDF/ZnO composite nanofibers using DSC, XRD and FTIR are presented in Sections 1 and 2 in the Supporting Information. A representative SEM image of PVDF/ZnO nanofibers (average diameters of 110 ± 35 nm) with 0.1 wt% ZnO is presented in Fig. 1b. The SEM images of PVDF/ZnO composite

nanofibers containing different amounts of ZnO are depicted in Fig. S3 (Supporting Information). The TEM images and SAED patterns of PVDF/ZnO nanofibers, Fig. S4 (Supporting Information) clearly demonstrate inclusion of the ZnO flakes inside the PVDF fibers. The V_{OC}, I_{SC} (Supporting Information Fig. S7c,d) and power density (Supporting Information Fig. S8) of the respective PNGs subjected to the same mechanical force of 20 N, are presented in Section 3 in the Supporting Information for impact frequency of 1 Hz. Incorporation of only 0.1 wt% ZnO into PVDF nanofibers, *viz.* sample Z0.1, increases the V_{OC} and I_{SC} values to 4.17 ± 0.09 V and 2.65 ± 0.04 μA, respectively. Further addition of ZnO beyond 0.1 wt%, however, suppresses the V_{OC} and I_{SC} of the PNGs. The power density delivered at the optimum load (Supporting Information Fig. S8) amounts to 74.60 ± 0.02 $\mu W/cm^3$ (at 1 Hz) for Z0.1 sample.

It has been demonstrated that PVDF forms β-phase crystallites on graphene [44]. Hence, to further enhance the power output, at the last step we fabricated PNGs by making a hybrid nanofiller of ZnO/rGO. Nanofibers of PVDF with 0.1 wt% of ZnO/rGO filler have been fabricated wherein the ZnO/rGO ratio is varied from 0 to 90/10 and 85/15. Details of the synthesis and characterization of the rGO and ZnO/rGO hybrids are given in Section 4 in the Supporting Information. Fig. 1c shows a representative SEM image of the resulting PVDF composite nanofibers with ZnO/rGO of 90/10 (average diameters of 122 ± 48 nm). The SEM image of ZG (85/15) sample is illustrated in Fig. S12 (Supporting Information). HR-TEM and hexagonal symmetry of the corresponding SAED of the fibers (Insets of Fig. 1c) demonstrate incorporation of ZnO decorated rGO sheets inside the PVDF nanofibers. Large rGO sheets are flexible and may be folded inside the fiber and form bead like structure, [42] as schematically shown in Fig. 1d.

DSC thermograms and FTIR spectra of the PVDF composite fibers containing hybrid fillers are presented in Fig. S13 (Supporting Information). The samples show dual melting peaks around 171-

175 °C, related to the simultaneous presence of both α and β polymorphs in the nanofibers [45,46]. Fig. 2a shows that the crystallinity, Xc, of the PVDF nanofiber is almost unchanged upon changing of the amount of rGO in the hybrid nanofiller, and remains at about 50%. However, the amount of the electroactive β-phase, F(β), substantially increases from ~68% for Z0.1 to 78% in the ZG (90/10) sample. Upon further increase of rGO in the hybrid nanofiller, *viz.* ZnO/rGO (85/15), the F(β) reduces to 73%. Reduction of F(β) could be ascribed to aggregation of rGO in the fibers at higher loadings, thus reducing β crystallinity of the composite fibers [47].

The comprising PNGs of the PVDF composite nanofiber with hybrid nanofillers *viz.* ZnO/rGO (90/10) and ZnO/rGO (85/15), show V_{OC} of 6.06 ± 0.08 V, 2.68 ± 0.05 V and I_{SC} of 3.46 ± 0.70 μA, 1.44 ± 0.05 μA, respectively, at an impact frequency of 1 Hz (Fig. 2b). Therefore, through optimization of the hybrid nanofillers, the PNG with ZnO/rGO (90/10) shows a V_{OC} that is nearly 10 times larger than that of the PNG made of pristine PVDF nanofibers, indicating the efficiency of the hybrid nanofiller compared to other used fillers, as illustrated in Table S1 (Supporting Information). To confirm that the output voltages are from the PNGs, polarity switching measurement has been conducted in the case of PNG made of ZG (90/10) sample. Fig. S14 (Supporting Information) demonstrates that the peak to peak V_{OC} value remains constant when the connection is reversed; however, opposite signals are generated. The sequence of curve ascending and descending is thoroughly reversed between forward and reverse connections.

The power-generating performance of the PNGs has also been evaluated by measuring the output voltages across various loading resistances. The power density at 1 Hz for the PNGs with ZnO/rGO compositions of (90/10) and (85/15), Fig. 2c,d, reaches to 138 ± 2.82 μW/cm^3 and 14 ± 0.65 μW/cm^3, respectively. Interestingly, the trend in power density matches the trend in the measured F(β). Table S2 (Supporting Information) demonstrates that our optimized PNG with ZnO/rGO

(90/10) nanofiller is among the PVDF-based PNGs with relatively high power densities, rendering the optimized PNG a potential candidate for realization of a self-powered cardiac pacemaker. In addition, recent advances have shown that PNGs based on lead-free piezoelectric materials have been developed with noticeable electric power [10,48-51] which can be considered as appropriate choices for power supply of pacemakers.

The superior performance of the optimized PNG can be attributed to the several factors. ZnO flakes and rGO sheets can induce β phase through interactions with PVDF. On one side, $-CH_2/-CF_2$ dipoles prefer to be oriented due to the hydrogen bonding between H atoms and functional groups of ZnO [52,53]. On the other side, the remaining functional groups of rGO tend to approach and interact with F atoms of PVDF [43,54]. As a consequence, the amount of β phase in PVDF composite fiber has increased, resulting in the improved piezoelectric output of the PNG.

Second, dipoles of PVDF are aligned in the piezoelectric β-phase due to the simultaneous application of mechanical stretching and the electric field during electrospinning, giving resultant potential difference between top and bottom electrodes of the PNG when the crystalline content of the fiber is impacted. [39]. Moreover, it has been suggested that due to the relative freedom of the polar nanoparticles, such as ZnO, in the solution of the composite, until solidification of the PVDF matrix of the nanofiber, the ZnO nanoparticles are free to rotate in the fiber so that they can align their polarization with the external electric field [53]. Hence, randomly aligned ZnO fillers in the solution, gradually align along the streamlines of the electric field during the electrospinning, producing a fully self-poled composite fiber [53]. It should be however noted that the experimental verification of the proposed mechanism is a daunting task, and is well beyond the scope of this manuscript.

Third, fillers in the PVDF composites act as stress concentration points when the PNG is under mechanical stress and enhance the piezoelectric output [55]. The generated electric potential (V) inside the PNG depends on the piezoelectric coefficient (d_{33}), thickness of the fiber mat (L), dielectric coefficient (ε), elastic constant (E), and the deformation along the vertical direction of the composite fiber (Y) [55]. Therefore, the electric potential can be stated as:

$$V = \frac{d_{33}\, E\, Y\, L}{\varepsilon} \quad (1)$$

Here, ZnO/rGO can reinforce the stress applied to the composite, leading to increased local deformation and larger generated piezoelectric output.

The piezoelectric coefficient (d_{33}) measurement also represents the ability of PNG to convert mechanical energy into an electric signal. In the case of fibers, d_{33} coefficient cannot be measured directly. Due to the porosity of the fiber mat and the presence of voids and air gaps in between the fiber network, the sample form electrical shorts upon electrode deposition, or suffer from dielectric break down of the air inclusions, rendering experimental d_{33} determination of the composite fibers challenging. Nevertheless, one may obtain an indication of the d_{33} values through calculating the number of generated charges, Q, upon application of an external force (F) using Equation (2) [56]. The charge generated upon the application of an applied force can be estimated by integrating the measured short circuit current, I_{SC}, of the resulting PNGs.

$$d_{33} = \frac{Q}{F} = \frac{\int I_{SC}\, dt}{F} \quad (2)$$

To arrive at a reliable estimate, and rule out experimental errors in the calculations, the calculated values can be normalized with respect to the fibers made of pristine PVDF. This procedure would allow us to compare relative increase/decrease in the d_{33} of the fibers. It has been concluded that the optimized composite fiber and PVDF composite fiber containing 0.1 wt% of ZnO/rGO (85/15) respectively show a nearly 12-fold and 5-fold increase in the d_{33} coefficient compared to pristine

PVDF fiber. Also, PVDF composite fibers containing 0.1 wt%, 1 wt%, 3 wt%, and 5 wt% of ZnO accordingly demonstrate a nearly 8-fold, 7-fold, 4-fold, and 2-fold increment in the d_{33} coefficient in comparison with pristine PVDF fiber. Table S3 (Supporting Information) compares the d_{33} values of various PVDF-based composites, confirming the high efficiency of ZnO/rGO hybrid filler used in our study.

The piezoelectric performance of the optimized PNG is also assessed in terms of the sensitivity parameter: S = V/P, where V and P are the open circuit voltage and applied mechanical pressure, respectively. The optimized PNG shows approximate sensitivity of 67.5 V/MPa under a load of 20 N and frequency of 1 Hz, which is higher than reported values of other PVDF-based PNGs, as shown in the Table S4 (Supporting Information). Hence, the optimized PNG is suitable for energy harvesting from minor movements of organs such as cardiac motions.

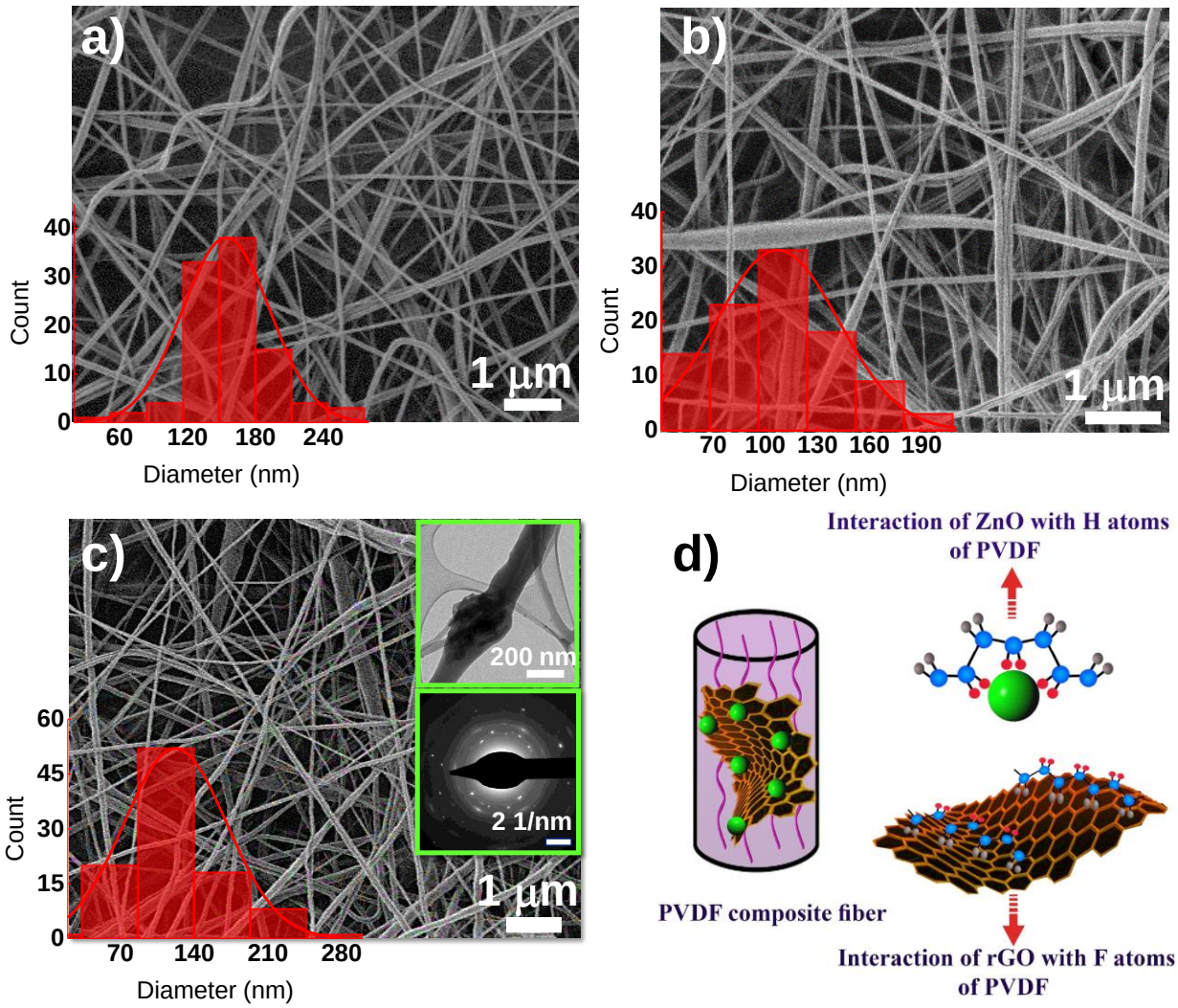

Fig. 1. a-c) SEM images and fiber diameter distribution of PVDF, Z0.1, and ZG (90/10) samples, respectively. Insets represent HR-TEM image and corresponding SAED pattern of ZG (90/10) sample. d) Schematic representing dispersion of hybrid nanofillers inside the PVDF NFs and formation of β-phase.

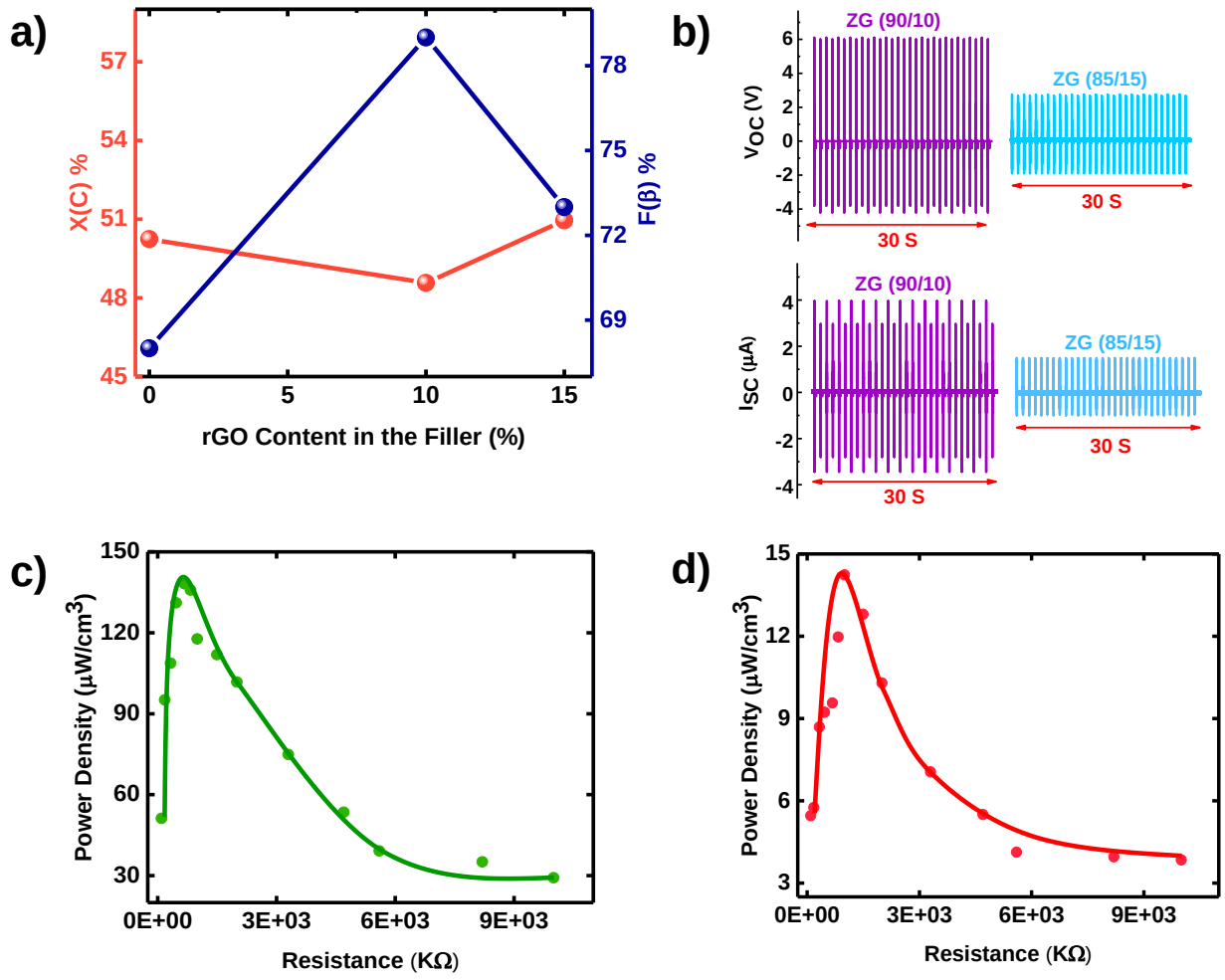

Fig. 2. a) Variation of crystallinity and β-phase content in hybrid composite fiber samples with rGO loading in the hybrid filler. b) V_{OC} and I_{SC} values of the ZG (90/10) and ZG (85/15) PNGs at frequency of 1 Hz under mechanically excitation of 20 N. c) Power density of ZG (90/10) and d) ZG (85/15) PNGs have been measured across a range of load resistances.

2.2. In vitro performance of the optimized PNG

As electrode, we have used Ag-coated Polydimethylsiloxane (PDMS) films. PDMS is used due to its excellent biocompatibility. Contacting with the PMDS layer also encapsulates the composite

fibers preventing penetration of water (body fluids) and thus provide leak-proof performance for the PNG, as schematically shown in Fig. 3a. The performance of the PNG before and after encapsulation for a PNG is illustrated in Fig. 3b. Upon encapsulation, the V_{OC} and I_{SC} of the PNG at the optimum load drop from 24.52 ± 1.11 V and 19.39 ± 1.08 μA to a V_{OC} and I_{SC} of 16.33 ± 1.11 V and 12.27 ± 2.65 μA, respectively. The higher output voltages (in comparison with data presented in Fig. 2) is simply due to the larger geometrical size of the devices [57]. The output power and power density for the PNG before encapsulation reach to 17 ± 1.47 μW and 257 ± 21.21 μW/cm^3, respectively, whereas for the encapsulated PNG the output power and power density accordingly drops to 4 ± 0.30 μW and 68 ± 2.82 μW/cm^3. Nonetheless, the output power is still large enough for the self-powered implantable heart pacemaker [13].

To confirm the stability of the PNG, we have conducted continuous mechanical impacting for the encapsulated PNG using the home-built device under the frequency of 1 Hz for one month. Fig. S15 (Supporting Information) shows that the V_{OC} and I_{SC} of the PNG do not reduce significantly upon repeated impacts for the whole month, indicating durability and stability of the PNG under prolonged mechanical impacting. The excellent durability of PNG confirms its capability as stable energy harvester for long-term usage.

2.3. Biocompatibility and cytotoxicity of the encapsulated PNG

To survey biosafety of the encapsulated PNG and PVDF fiber composite mat containing 0.1 wt% of ZnO/rGO (90/10) hybrid filler, we have performed *in vitro* biocompatibility tests. To that end, the adherence, growth and viability of MEF cells on the encapsulated PNG, composite fiber mat and cell culture dish have been performed and compared. Fig. 3c shows that MEF cells are adhered to all three samples with detectable cell nucleus. Results of MTT assay reveal that 98% and 96%

of the cells are viable after 3 days of culture, confirming good cytocompatibility of the designed PNG and composite fiber mat, respectively.

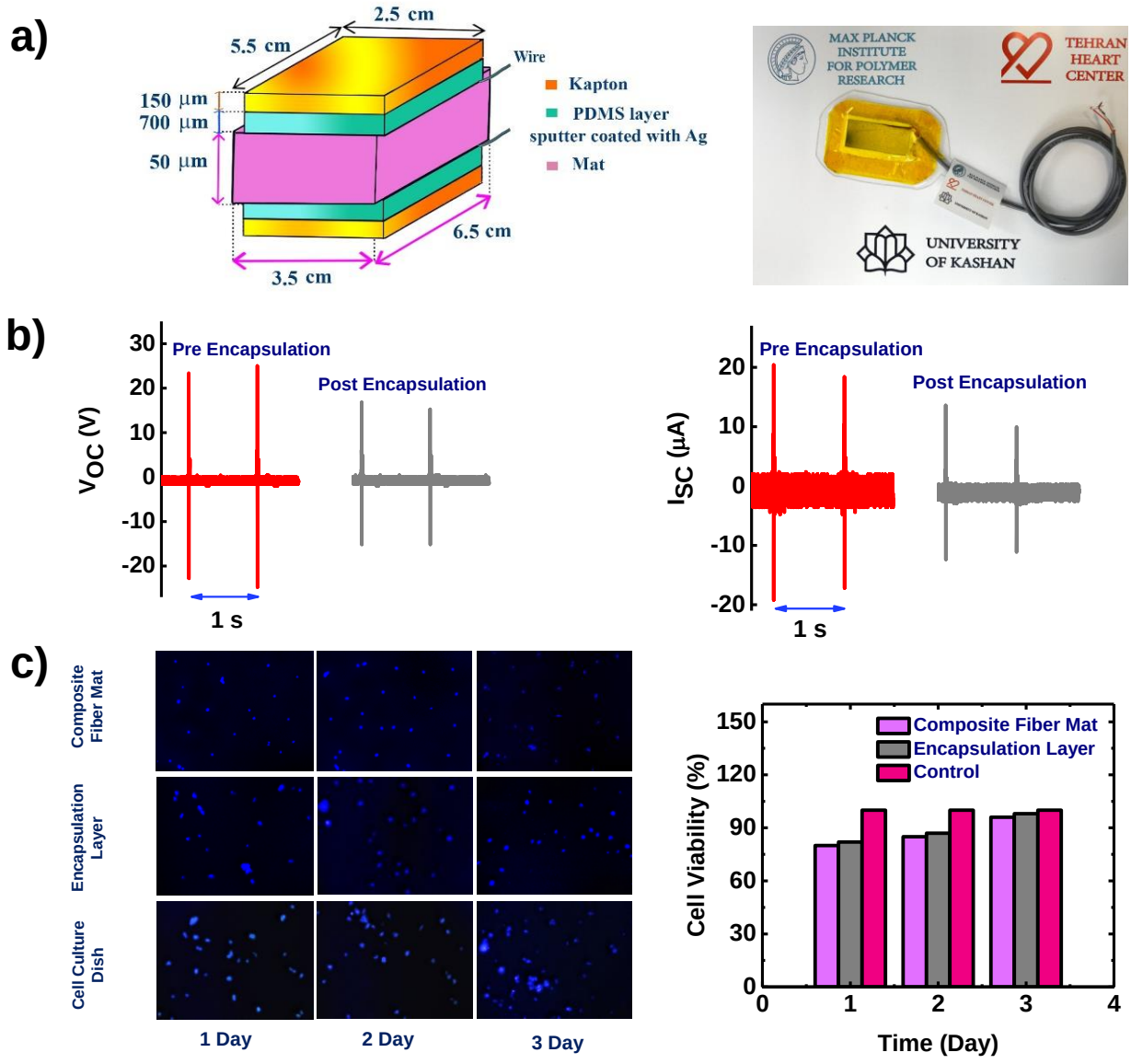

Fig. 3. a) Schematic and photograph of PNG. b) Open circuit voltage and short circuit current of PNG before and after encapsulation. c) Fluorescence images and viability of MEF cells after being

cultured on the composite fiber mat, encapsulation layer of the PNG, and cell culture dish for 1, 2, and 3 days.

2.4. In vivo implantation

To drive a cardiac pacemaker from the energy that is harvested from the implanted optimized PNG, *in vivo* experiment is performed on a large animal model with normal physiological activities, *i.e.* blood pressure of ~129/67 mmHg and heart rate of ~141 bpm (Fig. 4a-c). From physiological point of view, heart muscles contract in various directions, thus different deformations of heart such as tension, contraction, bending, and torsion are observed in a cardiac period [58]. Thus, the performance of energy harvester definitely relays on the location of the implanted PNG on the heart. The contractions of right and left ventricles (RV, LV) are more vigorous than the two atria, since they are separately responsible to pump two separated blood supplies to lungs and other organs, accordingly [12]. Between the two ventricles the LV has the largest motion amplitude and its maximum strain in systole is 35% larger than that of RV [59]. Considering these anatomic details, we have therefore placed the PNG on the lateral wall of LV. To fix the position, the PNG is sutured on the pericardium, facing the lateral LV wall.

During the *in vivo* implantation of the PNG, we have not used a rigid attachment in order to prevent any constraint on cardiac motion. The stitching, as shown in Fig. 4d, has been done on at the two far ends of the PNG to avoid disturbance on the heart function and to prevent injuries to the myocardium (Supporting Information Video S2). As shown in Fig. 4e, the PNG has not interfered with normal cardiac physiology and a typical/valid ECG has been detected during biomechanical energy harvesting by the PNG. Thus, we have inferred that the PNG has brought no burden to the

heart during the experiment. However, the implantation method needs additional improvements to keep the heart healthy during the lifespan of a patient.

After implantation of the PNG, the PNG has produced electrical voltage, synchronous with the heartbeat, as shown in the corresponding electrocardiography (ECG). Therefore, the measured piezoelectric voltage is associated to biomechanical impacting of PNG during systole and diastoles in the cardiac cycle. For every cycle, the PNG generates pulses as high as V_{OC} = 3.90 ± 0.65 V (and I_{SC} = 2.33 ± 0.62 μA at the optimum load) as shown in Fig. 4e. The generated voltage by the PNG is remarkably high and certainly higher than the maximum working voltage of a commercial battery driven cardiac pacemaker (2.8 V) [12]. We note that even a loose and un-sutured PNG is able to generate voltage during every cardiac cycle, thanks to the optimized performance of the PNG. As the PNG has been located on the heart without sutures, we have observed that the PNG has contact with the heart during the cycle of cardiac motion due to the large size of PNG (Supporting Information Video S1). Fig. S16a-c (Supporting Information) show that with every heartbeat, the PNG is able to harvest biomechanical energy from some local impacts and produce V_{OC} and I_{SC} of 1.39 ± 0.31 V and 0.90 ± 0.15 μA, respectively.

In order to demonstrate the *in vivo* long-term performance of the sutured PNG on the laboratory scale, the biomechanical energy harvesting capability of the PNG from heart motions has been evaluated during six hours. Fig. S17 (Supporting Information) illustrates the V_{OC} and I_{SC} of the PNG at various times of measurements. It is observed that the PNG does not show any significant reduction in the output voltage and current after six hours. To ensure the *in vivo* long-term performance of the PNG for actual medical applications, further assessments in prolonged period of time should be conducted in the future.

The sutured PNG harvests electrical energy as high as 0.487 μJ at the optimum load (Fig. 4f) during every cardiac cycle, which is larger than the energy that a typical commercial pacemaker (inset Fig. 4g) consumes (0.377 μJ) for cardiac sensing, adaptive pacing, and programmability [13,60]. The harvested energy is therefore sufficient to power a pacemaker. To that end, we have removed all the batteries inside a commercial pacemaker (inset Fig. 4g). The harvested energy from the heartbeats is stored in a 100 μF capacitor. The harvesting circuit is shown in Fig. S16d (Supporting Information). The charging curve of the storage capacitor is shown in Fig. 4g. The capacitor charges up to 3.5 V, in 323 minutes. Subsequently, the pacing leads of the pacemaker are connected to an oscilloscope. The pacemaker, as shown in Fig. 4h, generates pacing pulses of 3.1 ±0.1 V and a pulse width of 1.5 ms at the preset rate of 60 bpm (Supporting Information Video S3).

With the electric energy stored in the capacitor, we have powered a battery-free pacemaker for about 3 minutes. The harvested power of the PNG is typically stored in capacitors, which can be an issue due their fast discharge. To make full use of harvested energy and prolong the discharging time, commercial energy harvesting circuits such as ICs, LTC3385, and LTC3104 from linear technology, can be employed which ensure reliable and efficient power supplies at a defined voltage. Wang et al. [61] have also demonstrated that an optimized power management circuit can improve the efficiency of electrical energy harvesting.

It is worth noting that the successful performance of the polymer-based PNG in powering pacemaker is addressed here for the first time since it has not been investigated in previous studies. Besides, the present PNG has been shown to be improved in terms of biocompatibility and flexibility, compared to the ceramic-based biomechanical energy harvester [12,13,19,20] (Table

S5, Supporting Information). Such developments enable us to propose the PNG as an ideal power supply for the fabrication of self-powered pacemakers in the future.

In order to adopt the PNG for clinical application, some challenges need to be overcome. The PNG should be fabricated with the characteristic of long-term biosafety. Furthermore, to meet the requirement for a minimally invasive implantation, it is necessary to implant the PNG in accordance with medical protocols, for instance through efficient fixation using bio-tissues. Also, the PNG can be integrated with pacemaker design to generate electrical energy from mechanical motion of the pacemaker due to heart's contraction and relaxation. Such advances can be achieved in the future with the aid of materials science, micro/nano-fabrication skills, and electronics.

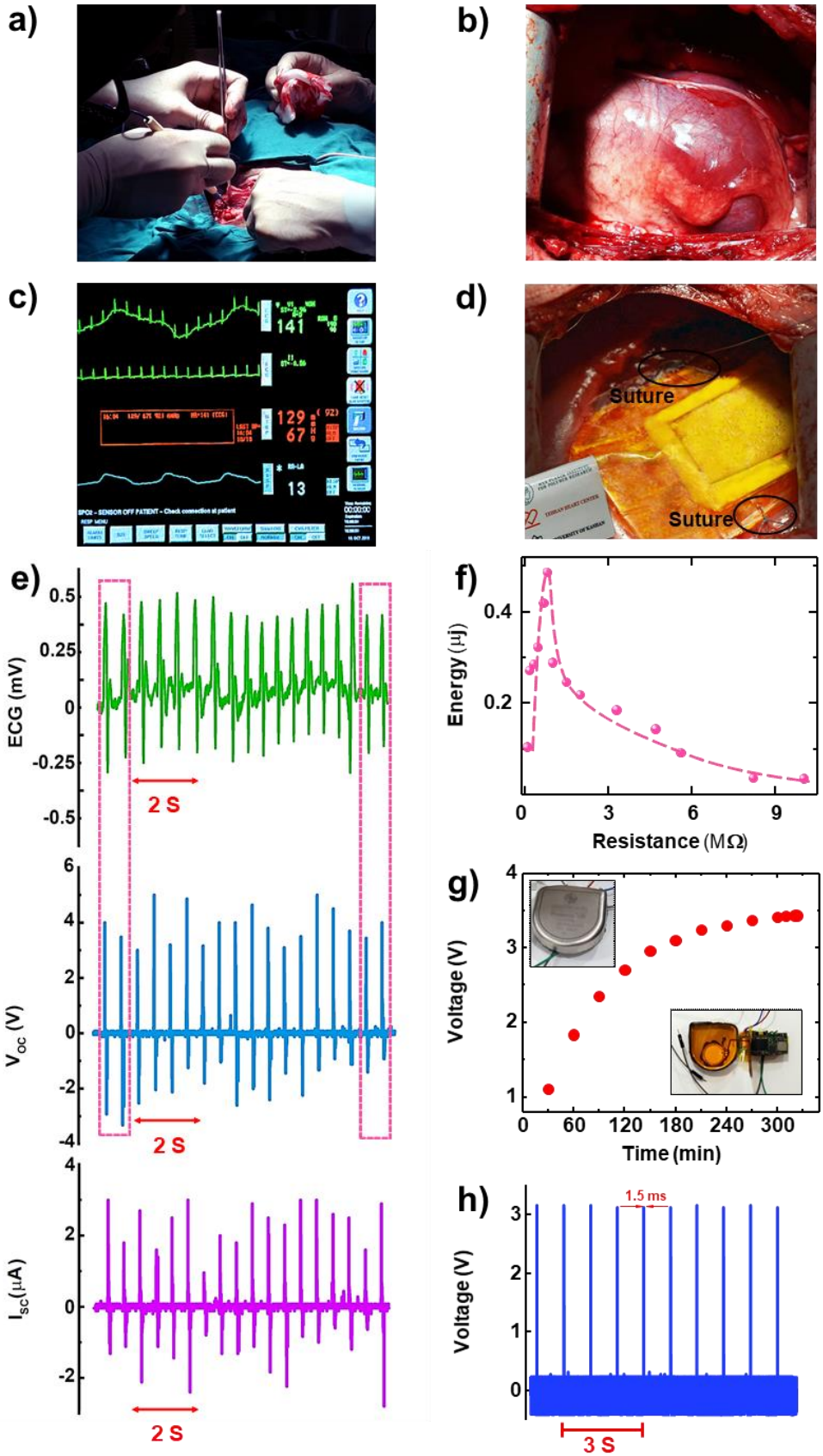
a)
b)
c)
d)
Suture
Suture
e)
ECG (mV)
2 S
V_{OC} (V)
2 S
I_{SC}(μA)
2 S
f)
Energy (μJ)
Resistance (MΩ)
g)
Voltage (V)
Time (min)
h)
1.5 ms
Voltage (V)
3 S

Fig. 4. Self-powered pacemaker. a) Surgery process in animal experiment. b) Photograph of the heart and c) simultaneously recorded ECG signals and blood pressure. d) The PNG sutured on epicardium facing lateral wall of LV. e) the in vivo open circuit voltage, corresponding ECG signal and short circuit current of the PNG. f) The generated energy of PNG measured across a range of load resistances through biomechanical energy harvesting of heart motions g) Charging curve of a 100 μF capacitor charged by the PNG. The top-left and bottom-right insets show the photograph of a commercial pacemaker, and the same after removal of the lithium battery, respectively. h) Generated pacing pulses by the pacemaker powered by the PNG.

3. Conclusions

In summary, we have reported a biocompatible and implantable polymer-based PNG that is optimized to harvest low frequency mechanical vibrations, and is used for the realization a self-powered pacemaker. The PNG has been optimized in multiple steps. A reliable large output power of 138 ± 2.82 $\mu W/cm^3$ is obtained for the PNG made of nanofibers of PVDF with only 0.1 wt% of ZnO/rGO (90/10) hybrid nanofillers. After the *in vivo* implantation on the lateral wall of the left ventricle of a dog animal model, the PNG has harvested electrical energy as high as 0.487 μJ from every heartbeat, which is larger than the pacing threshold in a commercial pacemaker. The *in vivo* energy harvesting of the PNG has powered a commercial pacemaker, generating pacing pluses at the preset parameters. Realization of a self-powered pacemaker can exempt the patients from surgeries for battery replacement, thereby improving the welfare of the patients. Furthermore, demonstration of an implantable PNG implies a significant step forward in providing sustainable power source for self-powered biomedical implants.

4. Material and methods

4.1. Materials

PVDF (Mw = 275000 g/mole, Mn = 107000 g/mole) was purchased from Solvay. Polydimethylsiloxane (PDMS) sylgard, Graphite powder, Potassium permanganate ($KMnO_4$), Sodium nitrate ($NaNO_3$), Zinc nitrate hexahydrate ($Zn(NO_3)_2.6(H_2O)$, Sodium hydroxide (NaOH), Cetyltrimethylammonium bromide (CTAB), Hydrazine hydrate, and Dimethyl formamide (DMF) were purchased from Sigma Aldrich, Inc. All chemicals were used as received.

4.2. Synthesis of ZnO

To synthesis ZnO flakes, 0.5063 g of $Zn(NO_3)_2.6(H_2O)$ was added to 30 mL deionized water, afterward 1 g NaOH was mixed to the solution while it was slowly stirred; subsequently, 1 g CTAB was added and stirred until a clear solution was obtained. The final mixture was transferred to a teflon-lined autoclave for hydrothermal synthesis at 120 °C. After 10 h the precipitated powder was collected and washed three times with deionized water and acetone, and dried at 80 °C.

4.3. Synthesis of rGO

GO was firstly obtained from natural graphite using Hummers method [62]. Then, the prepared GO was dispersed in de-ionized water and sonicated for 30 min. In the following, hydrazine hydrate was added and the solution was kept for 24 h at room temperature to obtain a black solution which was centrifuged and dried at 80 °C for 12 h to form rGO.

4.4. Synthesis of ZnO/rGO hybrid

To synthesize ZnO/rGO hybrids with amass ratio of 90/10 and 85/15, a specific amount of rGO was added to the ZnO dispersion in water, and the mixture was ultra-sonicated for 30 min. In order

to conduct the hydrothermal synthesis, the solution was transferred to a teflon-lined autoclave and kept at 120 °C for 10 h. The obtained precipitate was washed three times with deionized water and acetone and dried at 80 °C. For simplicity, the hybrids were referred as ZnO/rGO (90/10) and ZnO/rGO (85/15).

4.5. Electrospinning of PVDF-based composite fibers

Prior to making the electrospinning solutions, the nanofillers were dispersed in DMF and sonicated for 20 minutes. Subsequently. PVDF solutions in DMF containing different amounts of filler were prepared. The total solution concentration was kept at 20 wt%. After stirring at 60 °C overnight, the solution was ready for electrospinning. A voltage of 20 kV was applied to the needle, and a working distance of 15 cm, with feeding rate of 1 ml/h were the optimal operating conditions. A description of the samples is summarized in Table 1.

4.6. Scanning electron microscope (SEM)

Surface morphology of the samples was characterized using a Zeiss 1530 Gemini microscope. ImageJ processing software was utilized to measure the mean diameters of the fibers as well as the size of the fillers.

4.7. High resolution transmission electron microscope (HR-TEM)

The morphology of synthesized fillers and electrospun mats was imaged by a HR-TEM (FEI Tecnai F20) operated at 200 kV.

4.8. Attenuated total reflection Fourier transform infrared spectroscopy (ATR-FTIR) spectroscopy

ATR-FTIR spectra of the fibers were collected with an average of 64 scans in the range of 400-4000 cm^{-1} by a Bruker Tensor FT-IR Spectrometer + Platinium ATR Unit.

4.9. X-ray diffraction (XRD)

XRD patterns of the fillers and fibers were obtained using a diffractometer equipped with a monochromatic copper radiation source Cu K_α (λ= 1.5406 Å).

4.10. Differential scanning calorimetry (DSC)

The crystallinity of the fibers was determined using DSC. The samples were heated from 25 °C to 220 °C with heating rate of 10 °C/min under N_2 atmosphere using Mettler Toledo calorimeter.

4.11. PNG characterization

PNGs were fabricated by sandwiching a mat of the nanofibers with dimension of 1.5×1.5 cm^2 between two metal foils. Then, the PNGs were mechanically impacted at the frequencies of 1 Hz with impact force of 20 N using a home-built cyclic compression device. Open circuit voltage was measured using an oscilloscope. Short circuit currents were measured at different loads to calculate the optimum power.

4.12. Fabrication of biomedical implantable energy harvester

PDMS films were prepared by casting a degassed blend of PDMS (Sylgard 184, Dow Corning) and curing agent with the ratio of 10:1 and curing at 80 °C for 4 hours. Two flexible electrodes with dimensions of 5.5 by 2.5 cm and thickness of 700 μm were fabricated by sputter coating of Ag (300 nm) on the PDMS films. A piezoelectric mat with dimensions of 6.5 by 3.5 cm and thickness of 50 μm was cut and then sandwiched in between the electrodes using Kapton tape (150 μm). The whole assembly was again encapsulated in a PDMS layer.

4.13. Cell culture and biocompatibility

The mouse embryonic fibroblasts (MEF) were cultured with DMEM medium (1×), supplemented with 10% fetal bovine serum (Gibco) and 1% penicillin-streptomycin solution in a 75 cm^2 flask in a humidified atmosphere with 5% CO_2 and temperature of 37 °C. After 3 days, the cultured cells were seeded in 96-well plate on encapsulated PNG and PVDF composite fiber mat with 0.1 wt% of ZnO/rGO (90/10) filler. Then, the MTT (3-(4,5- dimethyldiazol-2-yl)-2,5-diphenyl tetrazolium bromid) assay was conducted to evaluate MEF cells viability. In brief, 100 μl of MTT solution was added to each well, followed by incubation for 3 h at 37 °C. Afterwards the MTT solution was aspirated, 100 μl of DMSO was added to each well and finally the optical densities (OD) of the samples were investigated on a spectrophotometer (Kontron Instruments) at 540 nm. The analytical test was performed after 24, 48 and 72 h.

4.14. Cell Morphology and immunofluorescent staining

DAPI was employed to stain the nucleus of MEF cells. The sample was fixed with paraformaldehyde 4% for 20 min and then rinsed three times with pre-warmed PBS (1×). Finally, the samples were incubated for 5 min at room temperature with DAPI. The morphology of the cells was imaged using inversion fluorescence microscope.

4.15. In vivo energy harvesting

An adult female dog (mixed-breed, weight: 25 kg) fasted for 12 hours without food and water prior to surgery. The dog received humane care in accordance with protocols of the Research Center for Advanced Technologies in Cardiovascular Medicine at Tehran Heart Center, Tehran University of Medical Sciences. All the procedures were performed with the permission from the ethics committee of Kashan University of Medical Sciences (IR.KAUMS.NUHEPM.REC.1396,21). In

brief, the animal was restrained with Ketamine Hydrochloride1 (10 mg/kg Intramuscular (IM)), weighed, and then Midazolam (1 mg/kg) was injected intravenously (IV) to relax the muscles. The animal was positioned in right recumbency and anesthetized with Thiopental Sodium (8mg/kg Intravenous (IV)) and 3-5% Isoflurane induction administered via an oral endotracheal tube (inhalation route). Anesthesia was maintained at 0.5-3% Isoflurane at room temperature throughout the study. Electrocardiogram (ECG) and blood pressure were monitored before and during the surgery. The thoracotomy was conducted on the left side, and cauterized with the electrosurgico knife. The fifth left intercostal space was opened and a retractor was used to expose the heart. Finally, the PNG was placed and sutured on the pericardium, facing the left ventricular wall. The PNG was then connected to the external circuit to measure the electrical outputs.

4.16. In vivo performance of PNG in powering pacemaker

To drive a commercial pacemaker (Medtronic Protecta VR, D364VRG) with the lithium battery being removed, the PNG was integrated with components in an electric circuit and the energy harvested from the heart motion was rectified and stored in a capacitor (100 μF). Then, the pacing leads of the pacemaker were connected to the oscilloscope to evaluate the pacing signals. When turned on by the wireless trigger of the Medtronic programmer, the stored electrical energy powered the pacemaker, producing pacing signals at the preset rate of 60 bpm.

Table 1. Description of PVDF-based composite fiber samples.

Sample Code	Filler	Filler wt% (with respect to PVDF weight)%
PVDF	No Filler	0
Z0.1	ZnO	0.1
Z1	ZnO	1
Z3	ZnO	3
Z5	ZnO	5
ZG (90/10)	ZnO/rGO (90/10)	0.1
ZG (85/15)	ZnO/rGO (85/15)	0.1

Acknowledgments

We thank the Max Planck Institute for Polymer Research for technical support. S.A. and M.M.A. would like to thank Kashan University of Medical Sciences for the financial support provided from research project number 96175. S.A. acknowledges Prof. Ezzat Rafiee and Dr. Elham Noori from Razi University, Iran for their helpful collaboration in synthesis of hybrid nanoparticles. M.H.A., M.M.A. and K. A. acknowledge the Alexander von Humboldt Foundation for the funding provided in the framework of the Sofja Kovalevskaja Award, endowed by the Federal Ministry of Education and Research, Germany. The authors are grateful to Prof. Paul W. M. Blom from the Max Planck Institute for Polymer Research for his support and the fruitful discussions.

References:

[1] K. Burney, F. Burchard, M. Papouchado, P. Wilde, Clin. Radiol. 59 (2004) 699-708.

[2] J. S. Perlmutter, J. W. Mink, Annu. Rev. Neurosci. 29 (2006) 229-257.

[3] G. Nelson, Tex. Heart Inst. J. 20 (1993) 12.

[4] G. T. Hwang, M. Byun, C. K. Jeong, K. J. Lee, Adv. Healthc. Mater. 4 (2015) 646-658.

[5] C. Liu, M. Peng, A. Yu, J. Liu, M. Song, Y. Zhang, J. Zhai, Nano Energy 26 (2016) 417-424.

[6] J. Chang, M. Dommer, C. Chang, L. Lin, Nano Energy 1 (2012) 356-371.

[7] S. Anwar, M. H. Amiri, S. Jiang, M. M. Abolhasani, P. R. F. Rocha, K. Asadi, Adv. Funct. Mater. (2020) 2004326.

[8] R. Wen, J. Guo, A. Yu, J. Zhia, Z. L. Wang, Adv. Funct. Mater. 29 (2019) 1807655.

[9] W. Liu, Z. Wang, G. Wang, G. Liu, J. Chen, X. Pu,Y. Xi, X. Wang, H. Guo, C. Hu, Z. L. Wang, Nat Commun. 10 (2019) 1-9.

[10]. Z. Hanani, I. Izanzar, M. Amjoud, D. Mezzane, M. Lahcini, H. Ursic, U. Prah, I. Saadoune, M. E. Marssi, I. A. Luk'yanchuk, Z. Kutnjak, M. Goune, Nano Energy 81 (2021) 105661.

[11] C. Dagdeviren, Z. Li, Z. L. Wang, Annu. Rev. Biomed. Eng. 19 (2017) 85-108.

[12] B. Lu, Y. Chen, D. Ou, H. Chen, L. Diao, W. Zhang, J. Zheng, W. Ma, L. Sun, X. Feng, Sci. Rep. 5 (2015) 16065.

[13] C. Dagdeviren, B. D. Yang, Y. Su, P. L. Tran, P. Joe, E. Anderson, J. Xia, V. Doraiswamy, B. Dehdashti, X. Feng, PNAS 111 (2014) 1927-1932.

[14] L. Dong, A. B. Closson, C. Jin, Y. Nie, A. Cabe, D. Escobedo, S. Huang, I. Trase, Z. Xu, Z. Chen, M. D. Feldman, J. X. J. Zhang, Adv. Healthc. Mater. 9 (2020), 2000053.

[15] L. Dong, C. Jin, A. B. Closson, I. Trase, H. R. Richards, Z. Chen, J. X.J. Zhang, Nano Energy 76 (2020) 105076.

[16] L. Dong, X. Han, Z. Xu, A. B. Closson, Y. Liu, C. Wen, X. Liu, G. P. Escobar, M. Oglesby, M. Feldman, Z. Chen, J. X. J. Zhang, Adv. Mater. Technol. 4 (2018) 1800148.

[17] Z. Xu, C. Jin, A. Cabe, D. Escobedo, N. Hao, I. Trase, A. B. Closson, L. Dong, Y. Nie, J. Elliott, M. Feldman, Z. Chen, J. X.J. Zhang, ACS Appl. Mater. Interfaces 12 (2020) 34170–34179.

[18] Z. Li, G. Zhu, R. Yang, A. C. Wang, Z. L. Wang, Adv. Mater. 22 (2010) 2534-2537.

[19] N. Li, Z. Yi, Y. Ma, F. Xie, Y. Huang, Y. Tian, X. Dong, Y. Liu, X. Shao, Y. Li, L. Jin, J. Liu, Z. Xu, B.Yang, H. Zhang, ACS Nano 13, (2019) 2822-2830.

[20] D. H. Kim, H. J. Shin, H. Lee, C. K. Jeong, H. Park, G.-T. Hwang, H.-Y. Lee, D. J. Joe, J. H. Han, S. H. Lee, J. Kim, B. Joung, K. J. Lee, Adv. Funct. Mater. 27 (2017) 1700341.

[21] W. Guo, C. Tan, K. Shi, J. Li, X. X. Wang, B. Sun, X. Huang, Y. Z. Long, P. Jiang, Nanoscale 10 (2018) 17751-17760.

[22] M. Baniasadi, J. Huang, Z. Xu, S. Moreno, X. Yang, J. Chang, M. A. Quevedo-Lopez, M. Naraghi, M. Minary-Jolandan, ACS Appl. Mater. Interfaces 7 (2015) 5358-5366.

[23] M. M. Abolhasani, M. Naebe, K. hirvanimoghaddam, H. Fashandi, H. Khayyam, M. Joordens, A. Pipertzis, S. Anwar, R. Berger, G. Floudas, J. Michels, K. Asadi, Nano Energy 62 (2019) 594-600.

[24] M. M. Abolhasani, S. Azimi, H. Fashandi, RSC Adv. 5 (2015), 61277-61283.

[25] M. M. Abolhasani, M. Ashjari, S. Azimi, H. Fashandi, Macromol. Chem. Phys. 217 (2016) 543-553.

[26] M. Baqeri, M. M. Abolhasani, M. R. Mozdianfard, Q. Guo, A. Oroumei, M. Naebe, J. Appl. Polym. Sci. 132 (2015) 42304.

[27] I. Katsouras, K. Asadi, M. Li, T. B. Van Driel, K. S. Kjaer, D. Zhao, T. Lenz, Y. Gu, P. W. Blom, D. Damjanovic, Nat. Mater. 15 (2016) 78-84.

[28] J. Martín, D. Zhao, T. Lenz, I. Katsouras, D. M. de Leeuw, N. Stingelin, Mater. Horiz. 4 (2017) 408-414.

[29] M. M. Abolhasani, M. Naebe, M. Hassanpour Amiri, K. Shirvanimoghaddam, S. Anwar, J. J. Michels, K. Asadi, Adv. Sci. 7 (2020) 2000517.

[30] M. M. Abolhasani, K. Shirvanimoghaddam, M. Naebe, Compos Sci Technol. 138 (2017) 49-56.

[31] M. M. Abolhasani, K. Shirvanimoghaddam, H. Khayyam, S. M. Moosavi, N. Zohdi, M. Naebe, Polym. Test. 66 (2018) 178-188.

[32] J. Fang, X. Wang, T. Lin, J. Mater. Chem. 21 (2011) 11088-11091.

[33] H. Fashandi, M. M. Abolhasani, P. Sandoghdar, N. Zohdi, Q. Li, M. Naebe, Cellulose 23 (2016) 3625-3637.

[34] C. Lee, D. Wood, D. Edmondson, D. Yao, A. E. Erickson, C. T. Tsao, R. A. Revia, H. Kim, M. Zhang, Ceram. Int. 42 (2016) 2734-2740.

[35] W. Zeng, X.-M. Tao, S. Chen, S. Shang, H. L. W. Chan, S. H. Choy, Energy Environl Sci. 6 (2013) 2631-2638.

[36] J. Briscoe, N. Jalali, P. Woolliams, M. Stewart, P. M. Weaver, M. Cain, S. Dunn, Energy Environl Sci. 6 (2013) 3035-3045.

[37] H. Parangusan, D. Ponnamma, M. A. A. Al-Maadeed, Sci. Rep. 8 (2018) 1-11.

[38] M. S. S. Bafqi, R. Bagherzadeh, M. Latifi, J. Polym. Res. 22 (2015) 130.

[39] S. Garain, S. Jana, T. K. Sinha, D. Mandal, ACS Appl. Mater. Interfaces 8 (2016) 4532-4540.

[40] X. Lu, H. Qu, M. Skorobogatiy, ACS Nano 11 (2017) 2103-2114.

[41] M. Pusty, A. Sharma, L. Sinha, A. Chaudhary, P. Shirage, ChemistrySelect 2 (2017) 2774-2782.

[42] K. Shi, B. Sun, X. Huang, P. Jiang, Nano Energy 52 (2018) 153-162.

[43] S. K. Karan, R. Bera, S. Paria, A. K. Das, S. Maiti, A. Maitra, B. B. Khatua, Adv. Energy Mater. 6 (2016) 1601016.

[44] K. L. Kim, W. Lee, S. K. Hwang, S. H. Joo, S. M. Cho, G. Song, S. H. Cho, B. Jeong, I. Hwang, J. H. Ahn, Nano lett. 16 (2016) 334-340.

[45] M. M. Abolhasani, M. Naebe, A. Jalali-Arani, Q. Guo, Nano 9 (2014) 1450065.

[46] M. M. Abolhasani, M. Naebe, A. Jalali-Arani, Q. Guo, PloS one 9 (2014) e88715.

[47] Y. Zhang, S. Jiang, Y. Yu, Y. Zeng, G. Zhang, Q. Zhang, J. He, J. Appl. Polym. Sci. 125 (2012) E314-E319.

[48] K. Il Park, S. Xu, Y. Liu, G. T. Hwang, S. J. L. Kang, Z. L. Wang, K. J. Lee, Nano Lett. 10 (2010) 4939-4943.

[49] W. Wu, L. Cheng, S. Bai, W. Dou, Q. Xu, Z. Wei, Y. Qin, J. Mater. Chem. A 1 (2013) 7332–7338.

[50] G. Zhu, R. Yang, S. Wang, Z.L. Wang, Nano Lett. 10 (2010) 3151-3155.

[51] R. Zhu, J. Jiang, Z. Wang, Z. Cheng, H. Kimura, RSC Adv. 6 (2016) 66451-66456.

[52] P. Thakur, A. Kool, N. A. Hoque, B. Bagchi, F. Khatun, P. Biswas, D. Brahma, S. Roy, S. Banerjee, S. Das, Nano Energy 44 (2018) 456-467.

[53] J. Li, S. Chen, W. Liu, R. Fu, S. Tu, Y. Zhao, L. Dong, B. Yan, Y. Gu, J. Phys. Chem. C. 123 (2019) 11378-11387.

[54] M. A. Rahman, G. S. Chung, J. Alloys. Compd. 581 (2013) 724-730.

[55] Y. Zhao, Q. Liao, G. Zhang, Z. Zhang, Q. Liang, X. Lia, Y. Zhang, Nano Energy 11 (2015) 719-727.

[56] A. Sultana, S. K. Ghosh, M. M. Alam, P. Sadhukhan, K. Roy, M. Xie, C. R. Bowen, S. Sarkar, S. Das, T. R. Middya, D. Mandal, ACS Appl. Mater. Interfaces 11 (2019), 27279-27287.

[57] S. He, W. Dong, Y. Guo, L. Guan, H. Xiao, H. Liu, Nano Energy 59 (2019) 745-753.

[58] R. Greenbaum, S. Y. Ho, D. Gibson, A. Becker, R. Anderson, Heart 45 (1981) 248-263.

[59] Z. Hu, D. Metaxas, L. Axel, Med Image Anal. 7 (2003) 435-444.

[60] P. Ritter, G. Z. Duray, C. Steinwender, K. Soejima, R. Omar, L. Mont, L. V. Boersma, R. E. Knops, L. Chinitz, S. Zhang, Heart J. 36 (2015) 2510-2519.

[61] X. Wang, P.R. Wilson, R. B. Leite, G. Chen, H. Freitas, K. Asadi, E. C. Smits, I. Katsouras, P. R. Rocha, Energy Technol. 8 (2020) 2000114.

[62] W. S. Hummers Jr, R. E. Offeman, J. Am. Chem. Soc. 80 (1958) 1339.